

Ultracold chemistry with alkali-metal-rare-earth molecules

C. Makrides,¹ J. Hazra,² G. B. Pradhan,² A. Petrov,^{1,*} B. K. Kendrick,³
T. González-Lezana,⁴ N. Balakrishnan,² and S. Kotochigova^{†1}

¹*Department of Physics, Temple University, Philadelphia, Pennsylvania 19122, USA*

²*Department of Chemistry, University of Nevada Las Vegas, Nevada 89154, USA*

³*Theoretical Division (T-1, MS B221), Los Alamos National Laboratory, Los Alamos, New Mexico 87545, USA*

⁴*Instituto de Física Fundamental, IFF-CSIC, Serrano 123, 28006 Madrid, Spain*

A first principles study of the dynamics of ${}^6\text{Li}({}^2\text{S})+{}^6\text{Li}^{174}\text{Yb}({}^2\Sigma^+)\rightarrow{}^6\text{Li}_2({}^1\Sigma^+)+{}^{174}\text{Yb}({}^1\text{S})$ reaction is presented at cold and ultracold temperatures. The computations involve determination and analytic fitting of a three-dimensional potential energy surface for the Li_2Yb system and quantum dynamics calculations of varying complexities, ranging from exact quantum dynamics within the close-coupling scheme, to statistical quantum treatment, and universal models. It is demonstrated that the two simplified methods yield zero-temperature limiting reaction rate coefficients in reasonable agreement with the full close-coupling calculations. The effect of the three-body term in the interaction potential is explored by comparing quantum dynamics results from a pairwise potential that neglects the three-body term to that derived from the full interaction potential. Inclusion of the three-body term in the close-coupling calculations was found to reduce the limiting rate coefficients by a factor of two. The reaction exoergicity populates vibrational levels as high as $v = 19$ of the ${}^6\text{Li}_2$ molecule in the limit of zero collision energy. Product vibrational distributions from the close-coupling calculations reveal sensitivity to inclusion of three-body forces in the interaction potential. Overall, the results indicate that a simplified model based on the long-range potential is able to yield reliable values of the total reaction rate coefficient in the ultracold limit but a more rigorous approach based on statistical quantum or quantum close-coupling methods is desirable when product rovibrational distribution is required.

PACS numbers: 34.50.Cx, 34.50.Lf, 82.20.Pm, 82.20.Xr

I. INTRODUCTION

Over the past several decades chemistry research has made large strides forward in the description of chemical reactions occurring in environments as diverse as combustion, the earth's atmosphere, and interstellar media where temperature and pressure vary over multiple orders of magnitude [1, 2]. Here, crossed molecular beam experiments have been instrumental in verifying and validating theoretical models of the reactions [3–5] that range from classical trajectory calculations, semiclassical theories and explicit quantum dynamics methods. The different theoretical approaches have been extensively reviewed in the literature [6–9]. However, these studies were mostly restricted to temperatures above 1 K where typically many angular momentum partial waves contribute to the overall rate coefficients. Only recently has it become possible to investigate chemical reactions between small molecules at temperatures well below 1 mK [10, 11] where quantum effects and threshold phenomena begin to dominate the collisional outcome. These novel capabilities pave the way to explore the fundamen-

tal principles of molecular reactivity at the very quantum limit, where a single collisional partial wave or mechanical-orbital angular momentum can dominate in the reaction. In fact, in many cases the collision has zero orbital angular momentum (except in collisions of identical fermions for which the lowest allowed partial wave is a p -wave), and thus has no centrifugal barrier.

Ultracold collisions between neutral alkali-metal atoms have been studied and quantified ever since the first laser cooling experiments of the late 1980s. Two of the most important outcomes were a thorough understanding of the non-classical scattering from the long-range dispersion potentials as well as the ability to significantly change the collision cross-section or scattering length with magnetic fields of the order of 100 G. This control of the scattering length is made possible by Feshbach resonances, weakly bound molecular states whose energy relative to that of the scattering atoms changes with magnetic field. Several excellent reviews were published on these topics recently, see Refs. [12–14]. On the other hand, reactions cannot occur in atomic collisions. State changing processes, however, are allowed. The electron or nuclear spin of the ground-state alkali-metal atoms can be reoriented converting a fraction of a kelvin of internal energy into kinetic energy.

While numerous theoretical predictions of ultracold chemical reactions have been reported since 2001 [15–18], controlled study of a chemical reaction with ultracold molecules started with the successful creation of a near

[†]Corresponding author: skotoch@temple.edu

*Alternative address: St. Petersburg Nuclear Physics Institute, Gatchina, 188300; Division of Quantum Mechanics, St. Petersburg State University, 198904, Russia.

quantum-degenerate gas of $^{40}\text{K}^{87}\text{Rb}$ molecules in their absolute ro-vibrational ground state at a temperature of a few hundred nanoKelvin by two JILA groups [10]. In this experiment an ensemble of ultracold fermionic ^{40}K atoms and bosonic ^{87}Rb atoms were bound together by transferring population from a Feshbach molecular state to the absolute ground state using a single optical Raman transition. Since these molecules were created in an optical trap they can collide among each other and with residual ultracold atoms and undergo chemical reaction, essentially at the single partial wave level.

The first measurement of the reaction rate coefficient between ultracold KRb molecules and K atoms was made at JILA [11]. The atom-molecule reaction rate coefficient was surprisingly high (on the order of $10^{-10} \text{ cm}^3/\text{s}$) even at temperatures below $1 \mu\text{K}$. Quantum defect theory (QDT) calculations [19, 20] showed that the reaction is nearly universal suggesting that the long-range van-der-Waals interaction plays a prominent role in the reaction dynamics. Recently, ultracold $^{87}\text{Rb}^{133}\text{Cs}$ molecules in their rovibrational ground state were produced at Innsbruck University [21]. These RbCs molecules are collisionally stable as atom exchange reactions to form homonuclear dimers are energetically forbidden [22].

They found that the former obeys the universal regime whereas departures from universality was noted for the latter. Explicit measurement of the reaction rate coefficient for the $\text{Li}+\text{CaH} \rightarrow \text{LiH}+\text{Ca}$ reaction was recently reported by Singh et al. at 1 K [23]. In this case, the buffer gas cooling method was employed for the CaH molecule that limits the translational temperatures to about 1 K.

A number of experimental groups around the world are working to create other alkali-metal and/or alkaline-earth molecules [24–28] in their stable ground states using a combination of magneto-association via Feshbach resonances and two-photon Raman photoassociation. Some of these molecules can undergo exothermic reactions, others are endothermic and need to be activated, for example by transfer to excited vibrational levels.

Both ultracold molecular experiments and theoretical modeling of collisions between alkali-metal and alkaline-earth molecules have focussed in total or integrated reaction rates. The next logical step is to measure and calculate final state resolved distributions. On the theory side this means using approaches that go beyond a “simple” universal QDT. In fact, a detailed understanding of the reaction mechanism and product rovibrational distribution requires a rigorous quantum treatment. While it is possible to combine such treatments with QDTs to yield full rovibrationally resolved reaction rate coefficients as demonstrated recently for the $\text{D}+\text{H}_2 \rightarrow \text{HD}+\text{H}$ reaction [29], additional efforts are needed for complex systems composed of alkali-metal and alkaline-earth metal systems.

Over the years researchers have identified several issues that can be used as guidelines to set up improved simulations. Chemical processes have been categorized by the presence or absence of a reaction barrier. Barrier-less

reactions are often described by capture theory, which suggests that their dynamics is principally controlled by the long-range potentials [30]. On the other hand, for some systems tunneling or coupling to a single scattering resonance or long-lived collisional complex dominates the reaction and advanced multi-channel QDT based on statistical interpretations may be applied [31, 32]. It is also important to understand the relative influence of the two- and three-body terms of the potential energy surfaces (PESs) on the collision dynamics. The three-body terms are influential when all three atoms are close together and fast moving, whereas two-body potentials dominate at long range, where at least one atom is far away. Naturally, one would like to understand whether these concerns affect reactions at very low temperatures. Using approximate quantum calculations based on knowledge of the long-range interactions, Mayle et al. [33, 34] predict that narrow resonances might dominate molecular collisions as a function of an applied electric field.

Finally, we note that in collisions between three- or more atoms there can exist intersecting PESs with the same symmetry, i.e. conical intersections [22, 35]. They are known to significantly affect reactions under the certain circumstances. For ground-state alkali-metal trimers intersecting PESs exist at the C_{2v} symmetry [22]. Moreover, at ultracold temperatures a full quantum dynamics calculation might need to include coupling between potential surfaces due to the hyperfine interactions between electronic and nuclear spins of the reactants. Several excellent reviews on chemical reactions of molecules at ultracold temperatures [18, 36] discuss these and some other questions.

The goal of this paper is to take an initial step toward addressing some of the questions raised above. In particular, we would like to compare the performance of universal models and statistical quantum-mechanical (SQM) approaches for ultracold reactions to a numerically exact quantum mechanical (EQM) method formulated in hyperspherical coordinates. We apply these approaches to the alkali-rare-earth LiYb molecule colliding with a Li alkali-metal atom at collisional energies E/k from $0.1 \mu\text{K}$ to 1 K, where k is the Boltzmann constant. These molecules can be created by photo/magnetoassociation from ultracold Li and Yb atoms and are the subject of on-going ultracold experiments [24, 37].

Quantum mechanical description of this reaction is challenging but simpler than alkali-metal system as there are no conical intersections. We ignore effects of the hyperfine interactions. Despite these simplicities, a full quantum calculation of this reaction is a computationally demanding task due to the high density of states of both LiYb and Li_2 molecules. For this reason, we restrict the EQM treatment to total angular momentum quantum number $J = 0$ (s-wave scattering in the initial LiYb channel) and adopt a J -shifting method [38] to evaluate temperature dependent rate coefficients. We hope to be able to transfer our insights from these studies to more complex systems composed of alkali metal and non-alkali

metal atom systems.

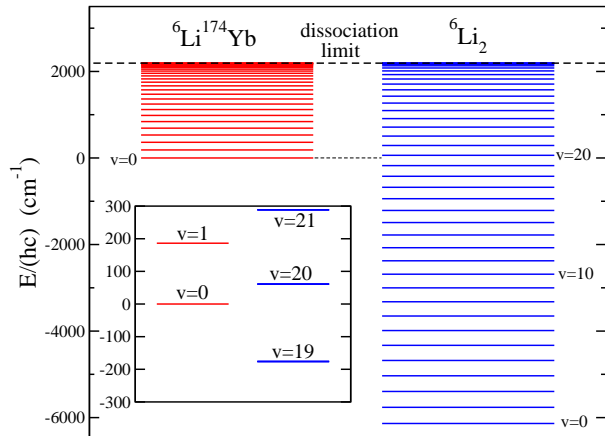


FIG. 1: Energetics of the $\text{LiYb}+\text{Li}\rightarrow\text{Li}_2+\text{Yb}$ reaction. The $j = 0$ vibrational levels of the $X^2\Sigma^+$ potential of the reactant ${}^6\text{Li}^{174}\text{Yb}$ molecule are shown on the left as horizontal red lines. The $j' = 0$ vibrational levels of the $X^1\Sigma_g^+$ potential of the product ${}^6\text{Li}_2$ molecule are shown on the right as horizontal blue lines. The zero of energy is located at the $v = 0$, $j = 0$ level of the ${}^6\text{Li}^{174}\text{Yb}$ molecule. (Energies are divided by Planck's constant h and the speed of light c .) The inset shows a blowup of the energy levels near the $v = 0$ level of ${}^6\text{Li}^{174}\text{Yb}$. For clarity the rotational progressions are not shown.

The paper is organized as follows. Section II describes our calculation of the ground-state LiYbLi trimer potential including a description of the interpolation between the *ab initio* points and the smooth connection to the long-range form of the potential. Section III describes a separate electronic-structure calculation of the dispersion potential between a LiYb molecule at its equilibrium separation and a Li atom. The dispersion coefficient is evaluated in terms of an integral over the dynamic polarizability of LiYb and Li as a function of imaginary frequencies [20, 39]. This coefficient is used in determining the reaction rate coefficients within the universal QDT treatment. Section IV describes the EQM, SQM, and universal calculations for the isotopes ${}^6\text{Li}$ and ${}^{174}\text{Yb}$. We present the results of these models in Sec. V. We also show a comparison of rate coefficients based on the full trimer potential and the pair-wise potential. Finally, state-to-state reaction rate coefficients derived from the SQM and EQM methods are analyzed and discussed. Summary and conclusion are presented in Sec. VI.

II. TRIMER POTENTIAL ENERGY SURFACE

The chemical reaction between a LiYb molecule and a Li atom is illustrated by the pathway



where initially the short-ranged, strong bond between the first $\text{Li}(1)$ atom and the Yb atom weakens as the second

$\text{Li}(2)$ atom approaches. An intermediate three particle “collision complex” $[\text{LiYbLi}]$ is formed. Finally, during the next stage of the reaction a short-range bond between $\text{Li}(1)$ and $\text{Li}(2)$ is formed and the Yb atom moves away quickly. The energetics of this reaction is shown in Fig. 1. The interaction potential of this reaction depends on three independent variables: the molecular bond lengths $R_{\text{Li}(1)\text{Yb}}$, $R_{\text{Li}(2)\text{Yb}}$, and $R_{\text{Li}(1)\text{Li}(2)}$ for the separation between $\text{Li}(1) + \text{Yb}$, $\text{Li}(2) + \text{Yb}$, and the two Li atoms, respectively.

The PES is an important part of the quantum dynamics calculations. No prior calculations exist on the PES for the $\text{LiYb}+\text{Li}$ reaction. We have computed the multi-dimensional ground-state potential surface of the “collision complex” by solving the Schrödinger equation for the electron motion with the nuclei held in fixed positions. Such calculations are computationally expensive as the energies of many molecular geometries are needed. We use the *ab initio* coupled-cluster method with single, double, and perturbative triple excitations (CCSD(T)) of the computational chemistry package CFOUR[40]. The trimer potential is improved by first subtracting the pair-wise, dimer potentials obtained at the same level of electronic structure theory. The remainder is the non-additive three-body potential $V^{(3)}(R_{\text{Li}(1)\text{Yb}}, R_{\text{Li}(2)\text{Yb}}, R_{\text{Li}(1)\text{Li}(2)})$. Earlier studies for the quartet potential of homonuclear and heteronuclear alkali-metal trimers [41–43] showed that non-additive effects are significant. An improved trimer potential is then created by adding the accurate experimental Li_2 ground state potential [44] and an *ab initio* theoretical LiYb potential determined with a larger basis set [45] to the three-body potential. No spectroscopic measurement of the LiYb potential exists at this time. This adjustment leads to the correct treatment of the long-range with at least one atom far away from the others. In section V we will compare reaction rate coefficients in the low-temperature regime based on the full trimer potential surface and to a pairwise-additive potential (which ignores the three-body potential).

For the coupled-cluster calculations we applied the aug-cc-pCVTZ basis set for the Li atom [46], whereas we chose a basis set constructed from the (15s 14p 12d 11f 8g)/[8s 8p 7d 7f 5g] wave functions of Dolg and Cao [47, 48] for the ytterbium atom. This ytterbium basis relies on a relativistic pseudopotential that describes the inner orbitals up to the $3d^{10}$ shell. Only, the 2s valence electrons of Li and $4f^{10}$ and $6s^2$ valence electrons of Yb are correlated in the *ab initio* calculation. The *ab initio* non-additive part of the trimer potential is fit to the generalized power series expansion of Ref. [49] given by

$$V^{(3)}(R_{\text{Li}(1)\text{Yb}}, R_{\text{Li}(2)\text{Yb}}, R_{\text{Li}(1)\text{Li}(2)}) = \sum_{i,j,k}^m d_{ijk} \rho_{\text{Li}(1)\text{Yb}}^i \rho_{\text{Li}(2)\text{Yb}}^j \rho_{\text{Li}(1)\text{Li}(2)}^k, \quad (2)$$

where the scaled length $\rho_{AB} = R_{AB}e^{-\beta_{AB}R_{AB}}$. The powers i , j , and k satisfy the conditions $i + j + k \leq m$,

$i + j + k \neq i \neq j \neq k$ for $m > 0$ to ensure that the potential goes to zero when one of the internuclear separations is zero [49]. The coefficients d_{ijk} and β_{AB} serve as linear and non-linear fit parameters, respectively, and are determined iteratively. Symmetry under interchange of the Li atoms ensures that $d_{ijk} = d_{jik}$ and $\beta_{\text{Li}(1)\text{Yb}} = \beta_{\text{Li}(2)\text{Yb}}$. For $m = 8$ we obtain a root-mean-square (rms) deviation smaller than $\delta V^{(3)} = 0.0004833$ a.u. for all 591 data points. The optimal 13 linear d_{ijk} and two non-linear β_{AB} coefficients are listed in Table I.

The advantage of the separation of the full potential into an additive and non-additive part is that the two-body pair-wise potentials can be replaced by either a more-advanced, high-precision electronic structure calculation or by an “experimental” potential that reproduces the binding energies of all-observed dimer ro-vibrational levels. In this paper we use the spectroscopically-accurate $X^1\Sigma_g^+$ potential for Li_2 [44] and our previously determined *ab initio* $X^2\Sigma^+$ potential for LiYb [45]. Both pair-wise potentials were expanded to large internuclear separation using the best-known van der Waals coefficients [50, 51]. The diatomic vibrational energies computed using these pair-wise potential curves are shown in Fig. 1. It is seen that the $\text{LiYb}(v = 0, j = 0) + \text{Li}$ reaction can populate vibrational levels as high as $v = 19$ of the Li_2 molecule at collision energies in the ultracold regime. A cut through our improved three-dimensional PES as a function of the LiYb and Li_2 bond lengths with the atoms restricted to a linear geometry is shown in Fig. 2. The reactant and product states are situated in the pairwise potential wells when either $R_{\text{Li}(1)\text{Li}(2)}$ or R_{LiYb} is large. We find that the optimized geometry, where the potential has its absolute minimum, occurs at this linear geometry with the three atoms on a line with the two Li atoms to one side (the same equilibrium configuration as

TABLE I: Parameters d_{ijk} and β_{AB} for the non-additive component of the three-body potential of LiYbLi as defined in the text. We have $\beta_{\text{LiYb}} = 0.7110242142956382$ and $\beta_{\text{LiLi}} = 0.2079741859771922$. Coefficients are in atomic units of the Hartree energy E_h and Bohr radius a_0 .

| i | j | k | d_{ijk} |
|---|---|---|---------------------|
| 1 | 0 | 1 | -0.3791234233645178 |
| 1 | 1 | 0 | -12.07092112030131 |
| 1 | 1 | 1 | 6.778574385332172 |
| 2 | 0 | 1 | 0.9609698323047215 |
| 2 | 1 | 0 | 18.08003175501403 |
| 0 | 1 | 2 | 0.4946458265430991 |
| 2 | 1 | 1 | -27.85537833078476 |
| 1 | 1 | 2 | 2.029448131083818 |
| 2 | 0 | 2 | -0.8786730695382046 |
| 2 | 2 | 0 | 104.7435507501138 |
| 3 | 0 | 1 | 0.07103760674735782 |
| 3 | 1 | 0 | 39.61820620689986 |
| 0 | 1 | 3 | -0.1402545726485475 |

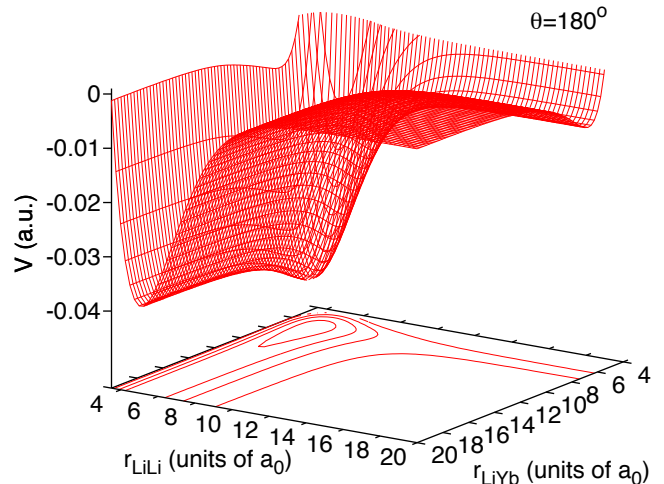


FIG. 2: A three-dimensional view of the PES in atomic units for the reaction $\text{Li}(1)\text{Yb} + \text{Li}(2) \rightarrow [\text{LiYbLi}] \rightarrow \text{Li}_2 + \text{Yb}$ as a function of bond lengths R_{LiYb} and $R_{\text{Li}(1)\text{Li}(2)}$. The angle between $R_{\text{Li}(1)\text{Li}(2)}$ and $R_{\text{Li}(2)\text{Yb}}$ is fixed at 180° . The zero of energy corresponds to the three separated atoms. Topographical contours of equal energies are shown on the base of the figure. From inside out their energies are $-0.04E_h$, $-0.03E_h$, $-0.02E_h$, and $-0.0075E_h$, respectively.

N_2O , for example). It occurs when $R_{\text{Li}(1)\text{Yb}} = 7.00a_0$, $R_{\text{Li}(2)\text{Yb}} = 12.25a_0$, and $R_{\text{Li}(1)\text{Li}(2)} = 5.25a_0$, respectively. In fact, the bond between the Li atoms is so strong that the Yb atom cannot get in between them and the Li-Li separation is close to that for the corresponding dimer potential. The atomization energy, the energy difference between the absolute minimum and three free atoms is $V_a = 0.045241$ a.u. (9929.0 cm^{-1}). The dissociation energy from the optimized geometry and the limit $\text{LiYb} + \text{Li}$ is $V_{d1}/(hc) = 0.0368949$ a.u. (8097.5 cm^{-1}), while that to the $\text{Li}_2 + \text{Yb}$ limit is $V_{d2}/(hc) = 0.007188$ a.u. (1577.6 cm^{-1}).

III. ATOM-DIMER DISPERSION POTENTIALS

In this section we determine the long-range dispersion potential for a polar LiYb molecule in the lowest vibrational level ($v = 0$) of the $X^2\Sigma^+$ potential and a lithium atom. We evaluate its isotropic and anisotropic contribution for rotation-less $j = 0$ and slowly-rotating $j = 1$ LiYb molecules. Later these coefficients will be used to evaluate universal reaction rates in Sec. IV C.

We calculate the atom-molecule van-der-Waals coefficients by integrating and summing the product of the LiYb and Li dynamic polarizability tensor $\alpha_{ij}(i\omega)$ over imaginary frequencies $i\omega$ and components i and j [39]. For polar molecules, which have a non-zero permanent dipole moment, there are contributions to the polarizability from ro-vibrational transitions within the ground-

state potential as well as those to excited electronic potentials. The contribution from transitions within the ground state is only important when the permanent dipole moment is large. For example, Ref. [20] showed that the ground-state contribution dominates for a heavy $v = 0$, $j = 0$ RbCs molecule and is small but non-negligible for the lighter KRb. The LiYb molecule has a very small permanent dipole moment of $0.011ea_0$ [45] at equilibrium separation $R_e = 6.71a_0$ and transitions to the electronically excited states dominate. Here, e is the charge of the electron.

The importance of excited electronic states in the calculation of the polarizability of vibrational ground state of LiYb allows us to make a simplification. We can neglect vibrational averaging and only have to determine the polarizability and thus the dispersion coefficients at R_e . Formally, the isotropic and anisotropic dispersion coefficients are [20, 39]

$$C_6^{\text{iso}} = \frac{3}{\pi} \int_0^\infty d\omega \bar{\alpha}^{\text{LiYb}}(i\omega, R_e) \bar{\alpha}^{\text{Li}}(i\omega) \quad (3)$$

and

$$C_{6,20}^{\text{aniso}} = \frac{1}{\pi} \int_0^\infty d\omega \Delta\alpha^{\text{LiYb}}(i\omega, R_e) \bar{\alpha}^{\text{Li}}(i\omega), \quad (4)$$

respectively, where for both atom and molecule $\bar{\alpha} = (\alpha_{xx} + \alpha_{yy} + \alpha_{zz})/3$ and $\Delta\alpha = \alpha_{zz} - (\alpha_{xx} + \alpha_{yy})/2$ in terms of the diagonal x , y , and z components of the polarizability tensor. For the molecule the components are in the body-fixed frame with z along the internuclear axis and $\alpha_{xx} = \alpha_{yy}$.

The diagonal dynamic polarizabilities $\alpha_{ii}^{\text{LiYb}}(\omega, R_e)$ are first calculated as a function of *real* frequency ω using the coupled-cluster method of CFOUR with single and double excitations (CCSD) [52]. The Li and Yb basis sets are the same as in the calculation of the trimer surface described in Section II. We then fit

$$\alpha_{ii}^{\text{Mol}}(\omega, R_e) = \sum_k \frac{A_k}{1 - (\omega/\eta_k)^2} \quad (5)$$

with parameters A_k and η_k . The A_k and η_k are related to the oscillator strength and transition frequency between ground and excited state k , respectively. We analytically continue to imaginary frequencies and perform the integral over frequencies to determine the dispersion coefficients.

Finally, we find that the isotropic C_6^{iso} coefficient for the $v = 0$ $X^2\Sigma^+$ LiYb molecule colliding with Li atom is $3086E_h a_0^6$ for both $j = 0$ and 1. The anisotropic $C_{6,20}^{\text{aniso}}$ coefficient is $776E_h a_0^6$ for the $j = 1$ molecule, while for the rotation-less $j = 0$ molecule it is zero. We verified that the contribution to C_6 from transitions within the ground state, to a good approximation is given by $d_e^4 / [(4\pi\epsilon_0)^2 6B_e]$ [53], where $B_e = 1.05 \times 10^{-6} E_h$ or $B_e/(hc) = 0.230 \text{ cm}^{-1}$ is the ${}^6\text{Li}^{174}\text{Yb}$ rotational constant at R_e and ϵ_0 is the electric constant, is negligible. The van der Waals length $R_{\text{vdW}} = (2\mu C_6^{\text{iso}}/\hbar^2)^{1/4}/2$ for the isotropic dispersion potential is $45.0a_0$ for ${}^6\text{Li}^{174}\text{Yb}$ and ${}^6\text{Li}$.

IV. QUANTUM DYNAMICS THEORY

In this and the following section we describe and compare the predictions of three scattering approaches of different levels of complexity. We begin with a description of each approach. In all three formalisms the effects due to the weak hyperfine and magnetic-field-induced Zeeman interactions of the Li atoms as well as any electric-field-induced level shifts of the polar LiYb molecule are omitted. For ground-state LiYb + Li collisions this implies that we only need to model couplings between the relative orbital angular momenta of the three atoms. In fact, the sum of these orbital angular momenta, the total angular momentum J and its space-fixed projection M , are conserved. Parity under spatial inversion, labeled by $p = \pm 1$, and particle exchange symmetry for identical particles within a diatomic molecule labeled by $q = \pm 1$ are also conserved quantities. Here, $q = \pm 1 = (-1)^{j'}$, corresponds to even and odd rotational levels j' of Li₂ [54]. The symmetries of the Hamiltonian ensure that the reaction rates are independent of M .

A. Exact quantum-mechanical method

The formalism for atom-diatom reactive scattering is well developed [8, 54–59]. Only a brief account relevant to the present context is provided here. We use the approach developed by Pack and Parker [58] based on the adiabatically adjusting principle axis hyperspherical (APH) coordinates (ρ, θ, ϕ) . This single-set of coordinates is convenient for the description of an atom-diatom chemical reaction as it evenhandedly describes all three arrangement channels, τ , in an A+BC system. On the other hand, one needs three sets of mass-scaled Jacobi coordinates $(S_\tau, s_\tau, \gamma_\tau)$ for describing chemical reaction [58]. Here, S_τ is the atom-molecule center-of-mass separation, s_τ is the diatom separation, and γ_τ is the angle between S_τ and s_τ . The hyper radius ρ is $\rho = \sqrt{S_\tau^2 + s_\tau^2}$, while expressions for the hyper angles θ and ϕ are given in Ref. [58]. Outside the region of strong interactions, where the three-body term has nearly decayed to zero, the three sets of Delves hyperspherical coordinates (DC), $(\rho, \theta_\tau, \gamma_\tau)$ are used where $\theta_\tau = \arctan(s_\tau/S_\tau)$ [55, 56]. The hyper radius in DC is the same as in APH but its hyper angles are defined differently and depend on the arrangement channel. In our approach, we adopt the APH coordinates (ρ, θ, ϕ) in the strong interaction region (inner chemically important region) and the DC $(\rho, \theta_\tau, \gamma_\tau)$ in the outer region. Finally, asymptotic boundary conditions are applied in Jacobi coordinates to evaluate the scattering matrix $S_{f \leftarrow i}^{J,pq}(E)$ for conserved J , p , and q . The indices i and f describe the initial and final scattering channels and E is the initial collision energy.

In the inner region, where APH coordinates are used,

the Hamiltonian for a triatomic system is

$$H = -\frac{\hbar^2}{2\mu\rho^5} \frac{\partial}{\partial\rho} \rho^5 \frac{\partial}{\partial\rho} + \frac{\hat{\Lambda}^2}{2\mu\rho^2} + V(\rho, \theta, \phi), \quad (6)$$

where $\mu = \sqrt{m_A m_B m_C / (m_A + m_B + m_C)}$ is the three body reduced mass, $\hat{\Lambda}$ is the grand angular momentum operator [60], and $V(\rho, \theta, \phi)$ is the adiabatic potential energy surface of the triatomic system. The total trimer wave function in this region for a given J, M, p , and q is expanded as [60–62]

$$\Psi^{JM,pq} = 4\sqrt{2} \sum_t \frac{1}{\rho^{5/2}} \Gamma_t^{J,pq}(\rho) \Phi_t^{JM,pq}(\Xi; \rho), \quad (7)$$

where the sum t is over five-dimensional (5D) surface functions $\Phi_t^{JM,pq}(\Xi; \rho)$ with $\Xi = (\theta, \phi, \alpha, \beta, \eta)$, where α, β , and η are Euler angles that orient the trimer in space. The other terms, $\Gamma_t^{J,pq}(\rho)$, are ρ -dependent radial coefficients. The orthonormal surface functions $\Phi^{JM,pq}(\Xi; \rho)$ depend parametrically on hyper radius ρ . For each ρ the surface functions are eigen solutions of the Hamiltonian $\hbar^2 \hat{\Lambda}^2 / (2\mu\rho^2) + V(\rho, \theta, \phi)$. To evaluate the 5D surface functions $\Phi_t^{JM,pq}(\Xi; \rho)$, we expand in terms of primitive orthonormal basis functions in Ξ given by $d_{\mu,\nu}^l(\theta) (e^{im\phi} / \sqrt{2\pi}) \tilde{D}_{\Omega M}^J(\alpha, \beta, \gamma)$, where $d_{\mu,\nu}^l(\theta)$ is expressed in terms of Jacobi polynomials $P_{l-\mu}^{(\mu-\nu, \mu+\nu)}(\cos\theta)$ [60], $\tilde{D}_{\Omega M}^J$ are normalized Wigner rotation matrices, and Ω is the projection of J on the body-fixed axis.

The basis function labels μ, ν, l and m can be integral or half-integral depending upon the value of total angular momentum J, Ω , and inversion parity p . [60] We introduce l_{\max} and m_{\max} where $\mu \leq l \leq l_{\max}$ and $|m| \leq m_{\max}$. The parameters l_{\max} and m_{\max} control the size of the basis sets in θ and ϕ . A hybrid discrete variable representation (DVR) in θ and a finite basis representation (FBR) in ϕ are used to solve the eigenvalue problem involving the surface function hamiltonian. An implicitly Restarted Lanczos Method (IRLM) of Sorensen [63] and Sylvester algorithm [64] are used for the diagonalization of the DVR Hamiltonian which includes tensor products of kinetic energy operators. Additionally, using a Sequential Diagonalization Truncation (SDT) technique [65, 66] the hamiltonian matrix is kept to a reasonable size.

Outside the region of strong interaction, we use DC and the total wave function is expanded in a complete set of ρ dependent vibrational wave functions $\Upsilon_n^{Jq}(\theta_\tau; \rho)$, coupled angular functions $\mathcal{Y}_n^{JM,pq}$, and radial functions $\Gamma^{J,pq}$ to yield

$$\Psi^{JM,pq} = 2 \sum_n \frac{1}{\rho^{5/2}} \Gamma_n^{J,pq}(\rho) \frac{\Upsilon_n^{Jq}(\theta_\tau; \rho)}{\sin 2\theta_\tau} \mathcal{Y}_n^{JM,pq}(\hat{S}_\tau, \hat{s}_\tau), \quad (8)$$

where n denotes collective molecular quantum numbers, $\{v_\tau, j_\tau, \ell_\tau\}$. The angles \hat{S}_τ and \hat{s}_τ are related to Euler angles via $d\hat{S}d\hat{s} = d\alpha \sin\beta d\beta d\eta \sin\gamma d\gamma$. The vibrational wave functions $\Upsilon_n^{Jq}(\theta_\tau; \rho)$ parametrically depend

on ρ and are computed using a one-dimensional Numerov propagator in θ_τ [67]. The Hamiltonian in the DC has the similar form as in APH except that the expression for $\hat{\Lambda}^2$ has a different form [67] and the variables of the three body PES are also different.

On substitution of $\Psi^{JM,pq}$ into the time-independent Schrödinger equation $H\Psi^{JM,pq} = E_{\text{tot}}\Psi^{JM,pq}$ one obtains a set of coupled equations in $\Gamma^{J,pq}(\rho)$. Using a sector-adiabatic approach in ρ , where ρ is partitioned into a large number of sectors, the surface functions are evaluated at the center of each sector. Assuming that the surface functions do not change within a sector, the solution of the Schrödinger equation is obtained by propagating the radial equations from a small value of ρ in the classically forbidden region to a large asymptotic value of $\rho = \rho_{\max}$. Here, we propagate the R-matrix $R(\rho) = \Gamma(\rho) (d\Gamma(\rho)/d\rho)^{-1}$ for each collision energy using the log-derivative method of Johnson [68]. Scattering boundary conditions are applied at ρ_{\max} to evaluate the scattering S-matrix. Details of the numerical integration, mapping between basis functions in the APH and DC coordinates, and asymptotic matching in Jacobi coordinates are given in Refs. [60, 67].

The S-matrix elements are used to calculate the partial reactive rate coefficient for a given J, p , and q ,

$$K_i^{J,pq}(E) = \frac{1}{2j_i + 1} v_r \frac{\pi}{k_r^2} \sum_f \left| S_{f \leftarrow i}^{J,pq}(E) \right|^2, \quad (9)$$

where the sum f is over all product (Li_2) ro-vibrational states (v_f, j_f) . In the usual way, we have also averaged over initial m_{j_i} and summed over all the final m_{j_f} . Here $v_r = \hbar k_r / \mu_{A,BA}$ is the incident relative velocity and $\hbar^2 k_r^2 / (2\mu_{A,BA}) = E$ is the relative kinetic energy in the incident channel with the reduced mass $\mu_{A,BA} = m_A(m_B + m_A) / (2m_A + m_B)$.

In order to construct the total reaction rate coefficient the role of the nuclear spin I of the two identical ${}^6\text{Li}$ nuclei must be considered. Following Ref. [54] we define symmetrized rate coefficient

$$\bar{K}_i^{J,pq}(E) = \frac{2I + 1 + q(-1)^{2I}}{2(2I + 1)} K_i^{J,pq}(E), \quad (10)$$

for a given p, q , and J and the total reaction rate coefficient becomes

$$K_i(E) = \sum_J (2J + 1) \sum_p \bar{K}_i^{J,pq}(E). \quad (11)$$

Since ${}^6\text{Li}$ has nuclear spin $I = 1$, this leads to weight factors $2/3$ and $1/3$ for even and odd ${}^6\text{Li}_2$ rotational levels j_f , respectively.

The EQM calculations involve the numerical computation of the 5D hyperspherical surface functions in the APH and DC and log-derivative propagation of the CC equation in these coordinates, followed by asymptotic matching to Li_2 and LiYb ro-vibrational states in Jacobi coordinates. We have restricted calculations for total angular momentum $J = 0$. For the inner region ranging

from $\rho = 6.0a_0$ to $33.89a_0$, the number of APH surface functions in θ and ϕ are controlled by l_{\max} and m_{\max} . For computational efficiency this hyperradial range was further divided into the three regions $6.0a_0 < \rho < 13.98a_0$, $13.98a_0 < \rho < 20.00a_0$, and $20.00a_0 < \rho < 33.89a_0$ with $l_{\max} = 119, 179, 399$ and $m_{\max} = 220, 280, 440$, respectively. For $J = 0$ this leads to 5D surface function matrices of dimension 52 920, 100 980, and 352 400. Fortunately, the dimensionality of these large matrices can be significantly reduced by using the SDT procedure to 23 986, 42 769, 136 489, leading to considerable savings in computational time. Furthermore, the explicit construction of these matrices is avoided by using an efficient sparse matrix diagonalization methodology (IRLM).

Finally, a logarithmic spacing in ρ is adopted with 88, 122 and 175 sectors, respectively. We compute 950 lowest energy surface functions for $J = 0$, leading to an equivalent number of coupled channel equations. Asymptotically, these channels correspond to different ro-vibrational levels of LiYb and Li₂ molecules. Among these, 636 are open channels and remaining 314 are closed channels.

Delves coordinates are used in the outer region comprised of $\rho = 33.89a_0$ to $\rho_{\max} = 107.48a_0$. A logarithmic spacing in ρ similar to that in the inner region is employed here. The number of basis functions in this region is controlled by an energy cutoff which is taken to be 0.9 eV relative to the minimum energy of the asymptotic Li₂ diatomic potential. As discussed previously, a one-dimensional Numerov method is used to compute the adiabatic surface functions $\Upsilon_n^{Jq}(\theta_\tau; \rho)$. Consequently, solution of the adiabatic problem in the Delves coordinates is fast compared to the APH part. The computational time for the log-derivative propagation of the radial equations is comparable to that in the inner region. We have verified that convergence of the scattering matrices was reached at $\rho_{\max} = 107.48a_0$ by comparing with results obtained at $\rho_{\max} = 118a_0$.

At $\rho = \rho_{\max}$, we match the DC wave functions to ro-vibrational levels of the LiYb and Li₂ molecules defined in Jacobi coordinates. This includes vibrational levels $v = 0 - 4$ for LiYb and $v' = 0 - 22$ for Li₂. For LiYb, rotational quantum numbers up to $j = 54, 47, 38, 27$ and 3 are incorporated in the vibrational levels $v = 0 - 4$ and for Li₂ rotational quantum numbers up to $j' = 101, 98, 95, 92, 90, 88, 85, 82, 79, 76, 73, 70, 66, 63, 60, 56, 52, 48, 43, 39, 33, 27$ and 17 are included in vibrational levels $v' = 0 - 22$, respectively.

B. Statistical quantum-mechanical method

The SQM has been developed to treat complex-forming atom-diatom reactions [31, 32, 69]. The method has been successfully employed in recent investigations of the low energy dynamics of the $D^+ + H_2 \rightarrow DH + H^+$ reaction [70–72]. In particular, statistical predictions were found in almost perfect agreement with both experimental and

quantum mechanical rate coefficients down to 11 K.

It assumes that the process proceeds via the formation of an intermediate three-body species between reactants and products with a sufficiently long lifetime. Consequently, the state-to-state reaction probability $P_{f \leftarrow i}^J(E)$, for conserved total angular momentum J and total energy E can be approximated by the product of the probability $p_i^J(E)$ of the complex to be formed from the initial reactant channel i and the fraction $p_f^J(E) / \sum_c p_c^J(E)$ of complexes fragmenting into the final product channel f (with Li₂ ro-vibrational state $v'j'\Omega'$) as follows:

$$P_{f \leftarrow i}^J(E) = \frac{p_i^J(E)p_f^J(E)}{\sum_c p_c^J(E)}. \quad (12)$$

The sum over c in Eq. (12) runs over all energetically open states, $E_c \leq E$, on both reactant and product channels at the total angular momentum J . To further simplify the SQM simulations we have used the centrifugal sudden (CS) approximation [69], where channel states are uniquely specified by the rovibrational quantum numbers v and j and projection Ω , where Ω is the body-fixed projection of the diatomic rotational angular momentum \vec{j} on the atom-diatom axis. For a collision energy of $E/k = 0.1$ K we have verified that a proper treatment of the Coriolis coupling between Ω states does not significantly modify the predicted rate coefficient.

The capture probabilities in each separate chemical arrangement τ are calculated as

$$p_c^J(E) = 1 - \sum_{c'} |S_{c' \leftarrow c}^J(E)|^2, \quad (13)$$

by solving the corresponding closed-coupled channel equations in radial Jacobi coordinate R_τ [31, 69] by means of a time-independent log-derivative propagator [73] between R_c , where the complex is assumed to form, and the asymptotic separation R_{\max} .

Finally, the total reaction rate coefficient for the ro-vibrational level vj of the LiYb molecule is given by

$$K_{vj}(E) = \sum_{v'j'} K_{v'j',vj}(E), \quad (14)$$

where the $vj \rightarrow v'j'$ state-to-state rate coefficient is

$$K_{v'j',vj}(E) = \frac{1}{2j+1} \sum_{J\Omega} \sum_{\Omega'} v_r(2J+1) \frac{\pi}{k_r^2} |S_{v'j'\Omega',vj\Omega}^J(E)|^2, \quad (15)$$

with $|S_{v'j'\Omega',vj\Omega}^J(E)|^2 = P_{f \leftarrow i}^J(E)$ and the sums over the body-fixed projections Ω' and Ω , as well as J and its space-fixed projection. The state-to-state rate is averaged over the $2j+1$ degenerate space-fixed projections of \vec{j} of the initial ro-vibrational level.

C. Universal model

The universal model (UM) is a further simplification of the reaction valid for the rotation-less $v = 0$ and

$j = 0$ LiYb molecule and ultracold collision energies. The model is based on a modification of the approach developed in Refs. [74, 75]. For sufficiently large separations $R > R_u$ between a rotation-less LiYb molecule and Li coupling to other ro-vibrational states is negligible and the long-range interaction potential is an attractive isotropic van-der-Waals potential $-C_6^{\text{iso}}/R^6$. Similar to the SQM we assume a scattering wavefunction that satisfies complete absorbing boundary conditions at the universal capture radius R_u . For these approximations to be valid the universal radius needs to satisfy the conditions $R_u \ll R_{\text{vdW}}$ and $C_6^{\text{iso}}/R_u^6 \sim 2B_e$, where B_e is the rotational constant of the $v = 0$ LiYb molecule. As an aside we note that the second condition ensures that $R_u \gg R_c$, as expected. The coefficient C_6^{iso} has been determined in Sec. III.

Under these assumptions the scattering of a rotation-less molecule with an atom is described by the single-channel potential $-C_6^{\text{iso}}/R^6 + \hbar^2 J(J+1)/(2\mu R^2)$, since for a $j = 0$ molecule the total angular momentum J of the trimer equals the relative orbital angular momentum between the atom and dimer. The corresponding Schrödinger equation with short-range boundary conditions is numerically solved for $R > R_u$ and the total reaction rate coefficient for collision energy E is given by

$$K_{v=0,j=0}^{\text{univ}}(E) = \sum_J (2J+1) v_r \frac{\pi}{k_r^2} (1 - |S_{\text{el}}^J(E)|^2), \quad (16)$$

where $S_{\text{el}}^J(E)$ is the elastic S-matrix element found by fitting the solution to in- and out-going spherical waves. Due to the absorbing boundary condition at $R = R_u$ we have $|S_{\text{elastic}}^J(E)| < 1$.

V. RESULTS AND COMPARISON

In this section we describe and discuss our results based on the three computational methods. We start with the EQM calculations. The upper panel of Fig. 3 shows the $J = 0$ EQM reactive rate coefficient for ${}^6\text{Li}^{174}\text{Yb}(v = 0, j = 0) + {}^6\text{Li}$ collisions as a function of the incident kinetic energy. Results are presented for even and odd rotational levels of diatomic Li_2 as well as for full three-body and additive pairwise potentials. The $J = 0$ results correspond to s -wave scattering in the incident channel and only s -waves contribute for energies below $100 \mu\text{K}$. The rate coefficients for the two potentials are similar for $E/k > 10^{-3}$ K, while significant differences are seen for lower energies with the zero-temperature rate coefficients differing by a factor of two. We also observe that the onset of the Wigner-threshold regime, where the rate coefficient approaches a constant for $E \rightarrow 0$, is shifted to slightly lower energies for the pairwise potential. This may be due to the slightly different bound-state spectrum of the Li_2Yb complex for the two PESs.

For collision energies $E/k > 10^{-3}$ K, non-zero angular momenta J need to be included. However, for our system this is not computationally feasible in the EQM

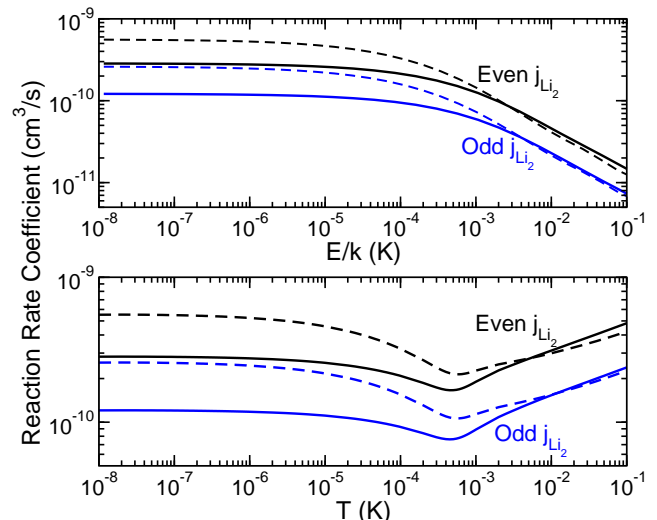


FIG. 3: Top panel) The EQM reaction rate coefficient for the collision of the $v = 0, j = 0$ ro-vibrational level of ${}^6\text{Li}^{174}\text{Yb}$ with a ${}^6\text{Li}$ atom as a function of relative collision energy E for total angular momentum $J = 0$. Lower panel) The thermally-averaged reaction rate coefficient summed over total angular momenta J using the J -shifting approach as a function of temperature T . In both panels black and blue lines correspond to rate coefficients to form even and odd rotational levels of the ${}^6\text{Li}_2$ product molecule, respectively. Solid and dashed lines are rate coefficients from calculations using the full trimer and the additive pair-wise potential, respectively.

approach. Instead, we adopt a J -shifting approximation [38], which was shown to work reasonably well for barrier-less reactions involving non-alkali metal atom systems. Details can be found in Ref. [61, 62]. In the lower panel of Fig. 3 we show the thermally-averaged reactive rate coefficients for full trimer and pairwise PES as a function of temperature evaluated using the J -shifting approach. Since the scattering calculation was only performed for collision energies up to 1 K, the Boltzmann average over collision energies limit the evaluation of the rate coefficient to temperatures up to 0.1 K. Results are presented for both even and odd rotational levels of the Li_2 molecule. For the full trimer potential, the rate coefficients in the zero-temperature limit for the even and odd Li_2 rotational levels are $2.61 \times 10^{-10} \text{ cm}^3/\text{s}$ and $1.11 \times 10^{-10} \text{ cm}^3/\text{s}$, while for the pairwise potential they are $5.33 \times 10^{-10} \text{ cm}^3/\text{s}$ and $2.49 \times 10^{-10} \text{ cm}^3/\text{s}$, respectively.

The EQM calculations allow the study of state-to-state reaction rates and, in particular, the distribution over the vibrational and rotational levels of the ${}^6\text{Li}_2$ molecule. Figure 4 plots the $J = 0$ rate coefficients to form ${}^6\text{Li}_2$ vibrational states (summed over all open rotational states) as a function of collision energy. The left and right panels correspond to the case when the full three-body and pair-wise potentials have been used, respectively. For both cases vibrational levels as high as $v' = 19$ are populated. The level $v' = 15$ is the most populated level for

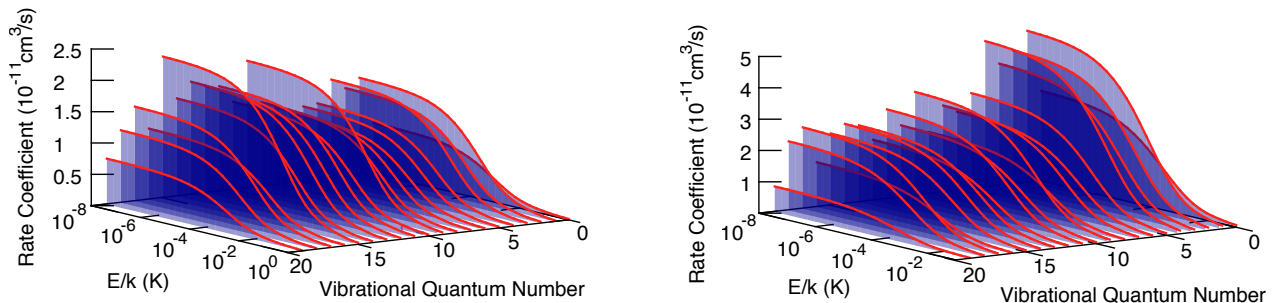


FIG. 4: The $J = 0$ state-to-state EQM reaction rate coefficient as a function of initial relative collision energy E and vibrational state of the ${}^6\text{Li}_2$ product molecule. Left panel correspond to the results based on the calculation with full trimer potential, whereas the right panel shows rate for the additive pair-wise potential.

the calculation with the full trimer potential, although vibrational levels $v'=1, 2, 3,$ and 9 are also comparably populated, indicating a broad range of vibrational excitation for the ${}^6\text{Li}_2$ product. On the other hand vibrational levels from $v'=1$ to $v'=4$ have a highest rate of population for the calculation with the pair-wise potential. Their rate coefficients are twice as high as those of the other vibrational levels.

Figures 5 and 6 show the $J = 0$ rate coefficients to form even and odd j' levels in the $v' = 15$ vibrational level of ${}^6\text{Li}_2$, respectively. In each figure the top and bottom panel correspond to collision energies $E/k = 10^{-4}$ K and 1 K, respectively, and rotational levels as high as $j' = 44$ are populated. Differently colored bars correspond to predictions for the full three-body and pair-wise potentials. For collision energies below 0.01 K (primarily the Wigner threshold regime), the relative distribution is independent of E .

For the full trimer potential the $v' = 15$ rate coefficients in Fig. 5 are dominated by the two highest rotational levels, $j' = 42$ and 44 . In other words, rotational levels, where the relative kinetic energy between the Li_2 dimer and Yb is smallest, are produced. On the other hand, the calculations with the pair-wise potential show the levels $j' = 22, 32,$ and 42 are most populated. At $E/k = 1$ K a broader range of rotational levels is populated with the highest population for $j' = 0$ and 26 for the full trimer potential and $j' = 0, 32$ and 38 for the pair-wise potential. Similar results have been observed for other barrier-less reactions involving non-alkali metal atom systems such as $\text{OH}+\text{O}$ and $\text{O}({}^1\text{D})+\text{H}_2$ [61, 62].

Figure 6 shows results for the rotational distribution of the odd j' levels in the $v' = 15$ vibrational level. At $E/k = 10^{-4}$ K calculations for the full trimer potential reveal that the $j' = 21$ and 41 levels are most populated, whereas for the pairwise potential these are the $j' = 3$ and 39 levels. At $E/k = 1$ K the population of $j' = 35, 37, 39$ and 41 dominates for the trimer potential and $j' = 19$ and $j' = 33$ levels for the pair-wise potential. Overall, the highly-excited rotational levels are

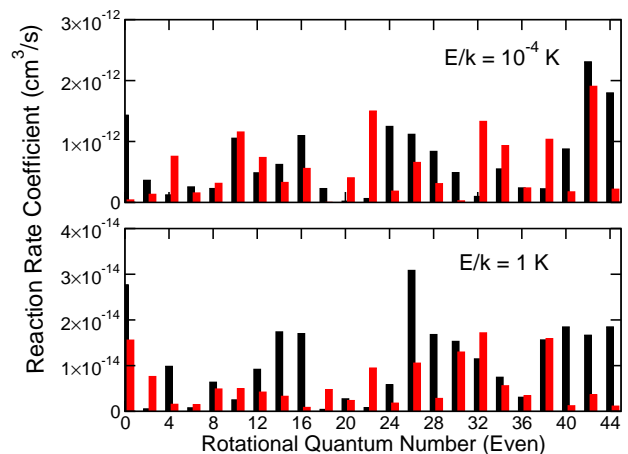


FIG. 5: The EQM reaction rate coefficient as a function of the even rotational quantum number of the $v' = 15$ vibrational level of the ${}^6\text{Li}_2$ molecule. The total angular momentum is $J = 0$. Upper and lower panels show the rate coefficient for an initial collision energy of $E/k = 10^{-4}$ K and 1 K, respectively. The black and red bars in both panels correspond to results of a calculation with the full trimer potential and additive pair-wise potential, respectively.

more populated than the lower rotational levels. This is partly driven by the anisotropy of the interaction potential and a compromise between conservation of internal energy and rotational angular momentum.

We now turn to describe the results obtained with the SQM method. In this study, the calculation for the $\text{LiYb}+\text{Li}$ reactant arrangement was performed for $R_c = 7a_0$ and a variable R_{max} depending on the energy under consideration, but with a largest value of $100a_0$, whereas for the Li_2+Yb product arrangement, those radii are $11.1a_0$ and $69.5a_0$, respectively. The selection of these values is made after numerical tests to guarantee the convergence of both individual capture, $p_i^J(E)$, and total, $P_{f \leftarrow i}^J(E)$, reaction probabilities. The SQM calculations in the reactants arrangement involves only the

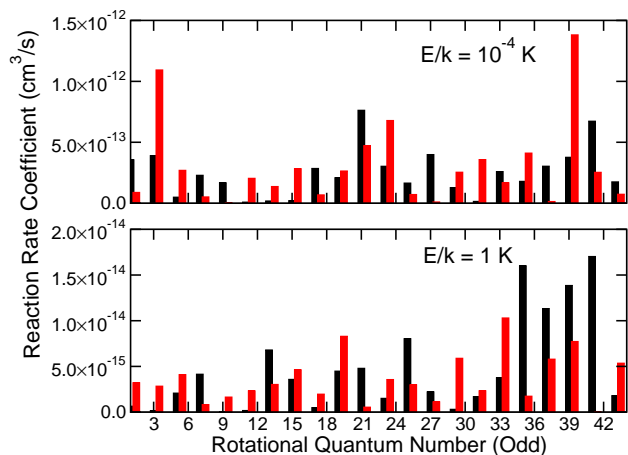


FIG. 6: The EQM reaction rate coefficient as a function of the odd rotational quantum number of the $v' = 15$ vibrational level of the ${}^6\text{Li}_2$ molecule. The total angular momentum is $J = 0$. Upper and lower panels show the rate coefficient for an initial collision energy of $E/k = 10^{-4}$ K and 1 K, respectively. The black and red bars in both panels correspond to results of a calculation with the full trimer potential and additive pair-wise potential, respectively.

LiYb ground vibrational state and rotational states up to $j = 16$, whereas in the product arrangement rovibrational states of the Li_2 molecule extend up to $v' = 16$ and $j' = 95$. Comparisons made at $E/k \sim 0.1$ K revealed that no significant differences are found between the CS approximation and a proper treatment of the Coriolis coupling term within the coupled-channel framework.

Figure 7 shows the SQM reaction rate coefficient to produce vibrational level $v' = 0 - 17$ of ${}^6\text{Li}_2$ as a function of collision energy E . The left panel shows the rate for $J = 0$, while the right panel includes sum over all J . The full trimer potential has been used in these calculations. The figure shows that the SQM calculation predicts rate coefficients that decrease with increasing v' . This contrasts the EQM data, which predict a far more complex v' dependence. This may be attributed to not accurately including the three-body forces in the SQM calculations. Experimental measurement of these state-to-state reaction rates are clearly needed. Ground state LiYb molecule does not exist yet.

The rotational dependence of the rate coefficient from SQM for three vibrational levels v' is shown Fig. 8. The number of j 's that can be populated follows from energy conservation and decreases with increasing v' . For small v' the j' dependence is fairly smooth and gently approaches zero for larger j' , while for higher v' more structure is predicted showing a maximum near the largest j' that are energetically accessible. For example, for $v' = 15$ rotational states around $j' = 40$ are most populated. These trends coincide with those predicted by EQM for the full trimer potential.

For ultracold molecular reactions the universal model (UM) has been very successful in qualitatively and some-

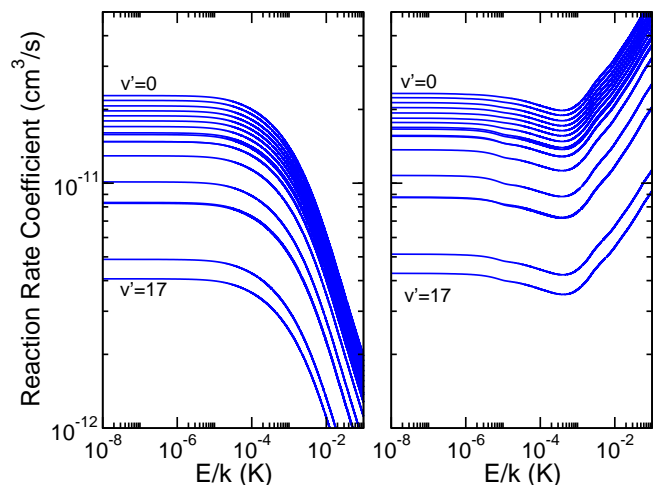


FIG. 7: The state-to-state SQM reaction rate coefficient for vibrational states v' of ${}^6\text{Li}_2$ as a function of relative collision energy. The left panel corresponds to the results restricted to total angular momentum $J = 0$ and right panel shows the rate coefficients summed over all J . The results are based on the full trimer potential.

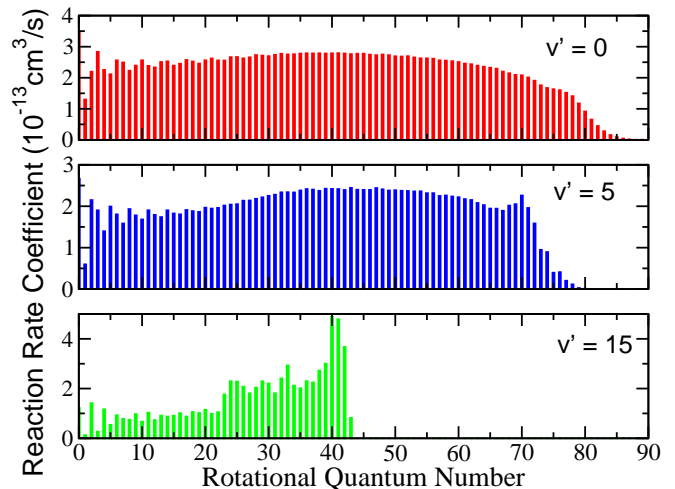


FIG. 8: The state-to-state SQM reaction rate coefficient for the rotational distribution in the $v' = 0$ (upper panel), $v' = 5$ (middle panel), and $v' = 15$ (lower panel) vibrational levels of the ${}^6\text{Li}_2$ molecule as a function of the rotational quantum number. The calculation is for $J = 0$ and $E/k = 10^{-4}$ K and is based on the full trimer potential.

times quantitatively describing the observed reaction rates [19, 20]. It solely depends on the dispersion coefficient between $\text{LiYb}(v=0)$ and Li and can only predict the total rate coefficient. In Fig. 9 we compare the UM rate coefficients for ${}^6\text{Li} + {}^6\text{Li}^{174}\text{Yb}(v=0, j=0)$ reaction with those of our other two calculations. For comparison purpose, the EQM results include contributions from both even and odd rotational levels of Li_2 . Results for both full trimer and pair-wise potential are given where appropriate.

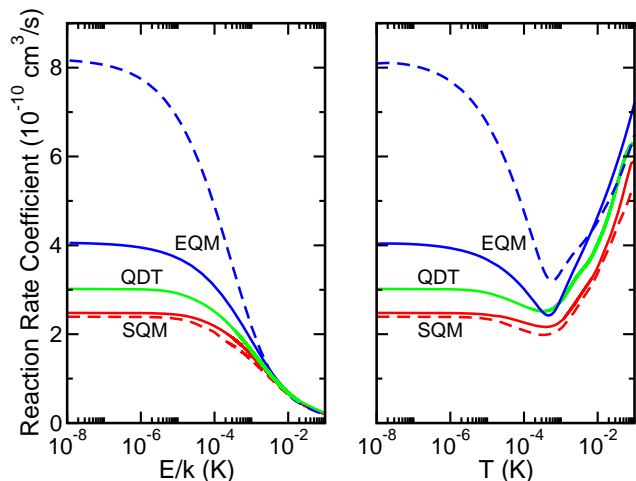


FIG. 9: The reaction rate coefficient for the $v = 0, j = 0$ ro-vibrational level of ${}^6\text{Li}^{174}\text{Yb}$ colliding with ${}^6\text{Li}$ as a function of collision energy, restricted to total angular momentum $J = 0$ (left panel) and the thermally-averaged rate coefficient summed over total angular momenta J as a function of temperature (right panel). The blue, red, and green curves correspond to the exact (EQM), statistical (SQM), and universal quantum-defect model (QDT), respectively. Solid and dashed lines for the EQM and SQM calculations correspond to calculations based on the full trimer potential and the pair-wise additive potentials, respectively. We used $C_6 = 3086 E_h a_0^6$ in the UM.

From the figure it is clear that results from different calculations with different potentials and varying degrees of approximations begin to merge for energies or temperatures above 10^{-3} K. Hence, the rate coefficient is largely insensitive to model and potential for collision energies above a mK. Rate coefficients from the SQM and UM models attain constant values for temperatures below 10^{-5} K in accordance with the Wigner threshold behavior. However, for the EQM results, this regime is attained only at about 10^{-5} K, presumably due to contributions from short-range interactions. This may also explain why the SQM results on the pair-wise additive and full trimer potentials yield comparable results. The SQM approach neglects most of the region of the potential between reactants and products where the intermediate complex is assumed to form. It is this region where specific features of the full potential are introduced but not fully taken into account in the SQM approach. The EQM results from the pair-wise additive and full trimer potentials show a factor of two difference in the ultracold regime, indicating sensitivity of results to fine details of the interaction potential. This is also evident from the product-resolved rate coefficients presented in Figs. 4, 5 and 6.

VI. CONCLUSION

We have investigated the chemical reaction between an ultracold LiYb molecule and an ultracold Li atom. This type of system was totally unknown in terms of its short- and long-range electronic potential surface as well as its scattering properties and reactivity. In this paper we reported on the first calculation of the ground-state electronic surface of the LiLiYb tri-atomic complex. We found that this collisional system possesses a deep potential energy surface that has its absolute minimum at a linear geometry with an atomization energy of 9929.0 cm^{-1} and accommodates many bound and quasi-bound states that are accessible in ultracold collisions making quantum dynamics simulations extremely challenging.

In addition, we performed a separate calculation of the long-range van der Waals potential between a Li atom and the LiYb molecule in the $v = 0$ vibrational level based on the dynamic polarizability of Li and LiYb. These van der Waals coefficients were used to estimate the universal reaction rate coefficient.

We explored the reactivity of this system at the quantum level using three different computational methods. These include an exact quantum mechanical method based on a rigorous close-coupling approach in hyperspherical coordinates that uses a minimal amount of assumptions. The EQM method predicts both total and state-to-state reaction rate coefficients, which we hope will stimulate the development of state-selective detection of the product molecules in ultracold reactions. This is one of the major challenges for ultracold chemistry in going beyond integrated reaction rate constants. The high accuracy of the reaction rates comes at the expense of model complexity and computational time.

We also explored two approximate quantum-mechanical methods to describe the reaction rate and capture the main features of the complex dynamics. One is the so-called statistical method, which assumes that the reactivity from reactants and products is controlled by one long-lived and short-ranged resonant state. The long-range scattering is described by separate coupled-channel calculations in Jacobi coordinates for the reactant (LiYb+Li) and product (Li₂+Yb) arrangements. This model makes predictions for state-to-state rate coefficients as well. Finally, we used the universal QDT model in the reactants arrangement, which assumes that at a carefully chosen separation between LiYb($v = 0, j = 0$) and Yb there is unit probability of a reaction. Reflection only occurs on the entrance-channel van der Waals potential. Consequently, this model does not depend on details of the strong short-ranged chemical interactions and only the total reaction rate coefficient can be calculated.

The total reaction rate coefficient as calculated from the three models agree for collision energies (or temperatures) above 10^{-3} K. Only for smaller collision energies and, in particular, in the Wigner threshold regime it differs by a factor of two. It was surprising for us to see

that in the Wigner threshold regime the universal model predicts a rate that lies between the EQM and SQM values. In the language of the universal model this suggests that there is a significant probability that flux is returned from the short-range region. The incoming and outgoing fluxes can then interfere. In EQM calculation these fluxes interfere in such a way that the reaction rate coefficient is significantly enhanced, whereas in the statistical model it is reduced. The disagreement between EQM and SQM in the Wigner threshold regime suggests that the underlying SQM assumption of a complex-forming dynamics for the reaction must be relaxed.

Both EQM and SQM calculations have been performed with the full three-body potential as well as the pair-wise potential. We conclude that only in the Wigner threshold regime with collision energies well below 10^{-3} K the EQM model is sensitive to the presence of the three-body contribution. On the other hand the SQM model shows no such sensitivity due to its neglect of three-body forces in the chemically important region.

Acknowledgments

The Temple University and UNLV teams acknowledge support from the Army Research Office, MURI grant No. W911NF-12-1-0476 and the National Science Foundation, grant Nos. PHY-1308573 (S.K.) and PHY-1205838 (N.B.). TGL acknowledges support from Project No. FIS2011-29596-C02-01 of the Spanish MICINN. BKK acknowledges that part of this work was done under the auspices of the US Department of Energy under Project No. 20140309ER of the Laboratory Directed Research and Development Program at Los Alamos National Laboratory. Los Alamos National Laboratory is operated by Los Alamos National Security, LLC, for the National Security Administration of the US Department of Energy under contract DE-AC52-06NA25396.

-
- [1] M. J. Howard and I. W. Smith, *J. Chem. Soc. Faraday Trans.* **2**, 997 (1981).
- [2] T. J. Millar and D. A. Williams, *Rate coefficients in astrochemistry* (Kluwer, Dordrecht, 1988).
- [3] D. M. Neumark, A. M. Wodtke, G. N. Robinson, C. C. Hayden, and Y. T. Lee, *J. Chem. Phys.* **82**, 3045 (1985).
- [4] M. Alagia, N. Balucani, P. Casavecchia, D. Stranger, G. Volpi, D. Clary, A. Kliesch, and H.-J. Werner, *Chem. Phys.* **207**, 389 (1996).
- [5] J. F. Castillo, B. Hartke, H.-J. Werner, F. J. Aoiz, L. Bañares, and B. Martínez-Haya, *J. Chem. Phys.* **109**, 7224 (1998).
- [6] G. Nyman and H. G. Yu, *Rep. Prog. Phys.* **63**, 1001 (2000).
- [7] S. C. Althorpe and D. C. Clary, *Annu. Rev. Phys. Chem.* **54**, 493 (2003).
- [8] W. Hu and G. C. Schatz, *J. Chem. Phys.* **125**, 132301 (2006).
- [9] H. Guo, *Int. Rev. Phys. Chem.* **31**, 1 (2012).
- [10] K.-K. Ni, S. Ospelkaus, M. H. G. de Miranda, A. Pe'er, B. Neyenhuis, J. J. Zirbel, S. Kotochigova, P. S. Julienne, D. S. Jin, and J. Ye, *Science* **322**, 231 (2008).
- [11] S. Ospelkaus, K.-K. Ni, D. Wang, M. H. G. de Miranda, B. Neyenhuis, G. Quémener, P. S. Julienne, J. L. Bohn, D. S. Jin, and J. Ye, *Science* **327**, 853 (2010).
- [12] T. Köhler, K. Góral, and P. Julienne, *Rev. Mod. Phys.* **78**, 1311 (2006).
- [13] C. Chin, R. Grimm, P. S. Julienne, and E. Tiesinga, *Rev. Mod. Phys.* **82**, 1225 (2010).
- [14] S. Kotochigova, *Rep. Prog. Phys.* **77**, 093901 (2014).
- [15] N. Balakrishnan and A. Dalgarno, *Chem. Phys. Lett.* **341**, 652 (2001).
- [16] R. V. Krems, *Int. Rev. Phys. Chem.* **24**, 99 (2005).
- [17] P. F. Weck and N. Balakrishnan, *Int. Rev. Phys. Chem.* **25**, 283 (2006).
- [18] G. Quémener, N. Balakrishnan, and A. Dalgarno, in *Cold Molecules: Theory, Experiment, Applications*, edited by R. V. Krems, W. C. Stwalley, and B. Friedrich (CRC Press Boca Raton, FL, 2009), chap. 3, p. 69.
- [19] Z. Idziaszek and P. S. Julienne, *Phys. Rev. Lett.* **104**, 113202 (2010).
- [20] S. Kotochigova, *New J. Phys.* **12**, 073041 (2010).
- [21] T. Takekoshi, L. Reichsöllner, A. Schindewolf, J. M. Hutson, C. R. de Sueur, O. Dulieu, F. Ferlaino, R. Grimm, and H.-C. Nägerl, arXiv:1405.6037 (2014).
- [22] P. S. Żuchowski and J. M. Hutson, *Phys. Rev. A* **81**, 060703(R) (2010).
- [23] V. Singh, K. S. Hardman, N. Tariq, M. J. Lu, A. Ellis, M. J. Morrison, and J. D. Weinstein, *Phys. Rev. Lett.* **108**, 203201 (2012).
- [24] H. Hara, Y. Takasu, Y. Yamaoka, J. M. Doyle, and Y. Takahashi, *Phys. Rev. Lett.* **106**, 205304 (2011).
- [25] M.-S. Heo, T. T. Wang, C. A. Christensen, T. M. Rvachov, D. A. Cotta, J.-H. Choi, Y.-R. Lee, and W. Ketterle, *Phys. Rev. A* **86**, 021602(R) (2012).
- [26] C.-H. Wu, J. W. Park, P. Ahmadi, S. Will, and M. W. Zwierlein, *Phys. Rev. Lett.* **109**, 085301 (2012).
- [27] T. A. Schulze, I. I. Temelkov, M. W. Gempel, T. Hartmann, H. Knöckel, S. Ospelkaus, and E. Tiemann, *Phys. Rev. A* **88**, 023401 (2013).
- [28] A. Khramov, A. Hansen, W. Dowd, R. J. Roy, C. Makrides, A. Petrov, S. Kotochigova, and S. Gupta, *Phys. Rev. Lett.* **112**, 033201 (2014).
- [29] J. Hazra, B. P. Ruzic, J. L. Bohn, and N. Balakrishnan, arXiv:1410.5873 (2014).
- [30] D. C. Clary, *Proc. Natl. Acad. Sci. USA* **105**, 12649 (2008).
- [31] E. Rackham, T. Gonzalez-Lezana, and D. E. Manopoulos, *J. Chem. Phys.* **119**, 12895 (2003).
- [32] T. González-Lezana, *Int. Rev. Phys. Chem.* **26**, 29 (2007).
- [33] M. Mayle, B. P. Ruzic, and J. L. Bohn, *Phys. Rev. A* **85**, 062712 (2012).
- [34] M. Mayle, G. Quémener, B. P. Ruzic, and J. L. Bohn,

- Phys. Rev. A **87**, 012709 (2013).
- [35] A. O. G. Wallis, S. A. Gardiner, and J. M. Hutson, Phys. Rev. Lett. **103**, 083201 (2009).
- [36] G. Quémener and P. S. Julienne, Chem. Rev. **112**, 4949 (2012).
- [37] A. H. Hansen, A. Khramov, W. H. Dowd, A. O. Jamison, V. V. Ivanov, and S. Gupta, Phys. Rev. A **84**, 011606(R) (2011).
- [38] J. M. Bowman, J. Phys. Chem. **95**, 4960 (1991).
- [39] A. J. Stone, *The Theory of Intermolecular Forces* (Clarendon Press, Oxford, 1996).
- [40] J. F. Stanton, J. Gauss, M. E. Harding, P. J. F. Stanton, J. Gauss, M. E. Harding, and P. G. Szalay, *CFOUR: A program package to perform high-level quantum chemical calculations on atoms and molecules* (2011).
- [41] P. Soldán, M. T. Cvitaš, J. M. Hutson, P. Honvault, and J.-M. Launay, Phys. Rev. Lett. **89**, 153201 (2002).
- [42] P. Soldán, M. T. Cvitaš, and J. M. Hutson, Phys. Rev. A **67**, 054702 (2003).
- [43] P. Soldán, Phys. Rev. A **82**, 034701 (2010).
- [44] B. Barakat, R. Bacis, F. Carrot, S. Churassy, P. Crozet, and F. Martin, Chem. Phys. **102**, 215 (1986).
- [45] S. Kotochigova, A. Petrov, M. Linnik, J. Klos, and P. S. Julienne, J. Chem. Phys. **135**, 164108 (2011).
- [46] B. P. Prascher, D. E. Woon, K. A. Peterson, T. H. Dunning, and A. K. Wilson, Theor. Chem. Acc. **128**, 69 (2011).
- [47] X. Cao and M. Dolg, J. Chem. Phys. **115**, 7348 (2001).
- [48] M. Dolg (2013), private Communication.
- [49] A. Aguado and M. Paniagua, J. Chem. Phys. **96**, 1265 (1992).
- [50] M. S. Safronova, S. G. Porsev, and C. W. Clark, Phys. Rev. Lett. **109**, 230802 (2014).
- [51] Z.-C. Yan, J. Babb, A. Dalgarno, and G. Drake, Phys. Rev. A **54**, 2824 (1996).
- [52] M. Kallay and J. Gauss, J. Mol. Struct. (Theochem) **768**, 71 (2006).
- [53] R. Barnett, D. Petrov, M. Lukin, and E. Demler, Phys. Rev. Lett. **96**, 190401 (2006).
- [54] W. H. Miller, J. Chem. Phys. **50**, 407 (1969).
- [55] L. M. Delves, Nucl. Phys. **9**, 391 (1959).
- [56] L. M. Delves, Nucl. Phys. **20**, 275 (1960).
- [57] B. Lepetit, J. M. Launay, and M. Le Dourneuf, Chem. Phys. **106**, 103 (1986).
- [58] R. T. Pack and G. A. Parker, J. Chem. Phys. **87**, 3888 (1987).
- [59] J. M. Launay and M. Le Dourneuf, Chem. Phys. Lett. **163**, 178 (1989).
- [60] B. K. Kendrick, R. T. Pack, R. B. Walker, and E. F. Hayes, J. Chem. Phys. **110**, 6673 (1999).
- [61] G. B. Pradhan, N. Balakrishnan, and B. K. Kendrick, J. Chem. Phys. **138**, 164310 (2013).
- [62] G. B. Pradhan, J. C. Juanes-Marcos, N. Balakrishnan, and B. K. Kendrick, J. Chem. Phys. **139**, 194305 (2013).
- [63] D. C. Sorensen, SIAM J. Matrix Anal. Appl. **13**, 357 (1992).
- [64] D. Hu and D. Sorensen, Tech. Rep. TR94-10, Rice University (1994).
- [65] Z. Bačić, R. M. Whitnell, D. Brown, and J. C. Light, Comput. Phys. Commun. **51**, 35 (1988).
- [66] Z. Bačić, J. D. Kress, G. A. Parker, and R. T. Pack, J. Chem. Phys. **92**, 2344 (1990).
- [67] G. A. Parker, R. B. Walker, B. K. Kendrick, and R. T. Pack, J. Chem. Phys. **117**, 6083 (2002).
- [68] B. R. Johnson, J. Comput. Phys. **13**, 445 (1973).
- [69] E. J. Rackham, F. Huarte-Larrañaga, and D. E. Manolopoulos, Chem. Phys. Lett. **343**, 353 (2001).
- [70] T. González-Lezana, Y. Scribano, and P. Honvault, J. Phys. Chem. A **118**, 6416 (2014).
- [71] T. González-Lezana and P. Honvault, Int. Rev. Phys. Chem. **33**, 371 (2014).
- [72] T. González-Lezana, P. Honvault, and Y. Scribano, J. Chem. Phys. **139**, 054301 (2013).
- [73] D. E. Manolopoulos, J. Chem. Phys. **85**, 6425 (1986).
- [74] F. H. Mies, J. Chem. Phys. **80**, 2514 (1984).
- [75] P. S. Julienne and F. H. Mies, J. Opt. Soc. Am B **6**, 2257 (1989).